Geophysical Research Letters

Supporting Information for

Positive Low Cloud Feedback Primarily Caused by Increasing Longwave Radiation from the Sea Surface in Two versions of a Climate Model

Tomoo Ogura[1], Mark J. Webb[2], and Adrian P. Lock[2]

[1]National Institute for Environmental Studies, Tsukuba, Japan

[2]Met Office Hadley Centre, Exeter, United Kingdom

Contents of this file

Texts S1-S2, Figures S1-S11, Table S1

Introduction

This document contains additional text, figures, and a table which support arguments in the main text.

Text S1. Experimental design

In MIROC5 and MIROC6, SST warming influences the atmosphere through changes in two factors. One is the upward longwave radiation emitted from the sea surface, and the other is the turbulent transport of heat, moisture, momentum, and aerosol from the sea surface. Without any changes in the two factors, the SST warming cannot influence the model atmosphere.

In the AMIP-p4K experiment, the SST warming changes both the two factors to influence the atmosphere. In the AMIP-p4Krad or the AMIP-p4Kturb experiment, the SST warming changes either one of the two factors to influence the atmosphere. Here we describe how the AMIP-p4Krad and AMIP-p4Kturb experiments are implemented.

1. AMIP-p4Krad experiment

In MIROC5 and MIROC6, upward longwave radiation that is emitted from the surface of the land or ocean is calculated from the surface temperature, T_{s_rad}, using Planck's function. This upward longwave radiation causes heating at multiple atmospheric layers above the surface.

In the AMIP experiment, we prescribe SST as a boundary condition, which is used as the input variable T_{s_rad} to calculate the upward longwave radiation emitted from the sea surface. In the AMIP-p4Krad experiment, we add 4K to the T_{s_rad} at the sea surface. The experimental setting of the AMIP-p4Krad is the same as the AMIP, other than adding 4K to the T_{s_rad}.

The 4K warming of T_{s_rad} causes an increase in upward longwave radiation emitted from the sea surface, which leads to an increase in radiative heating at multiple atmospheric layers above the surface (Figure 3i). As a result, the atmospheric temperature increases, which is prominent in the lower troposphere (red curve in Figure 3h).

2. AMIP-p4Kturb experiment

Turbulent transport of sensible heat, latent heat, and momentum from the surface to the atmosphere is calculated using the bulk aerodynamic formulas in the MIROC5 and MIROC6. The formulas are defined as follows.

$$SH = \rho \cdot C_p \cdot C_{DH}(T_{s\_turb}) \cdot |\vec{V}| \cdot \{T_{s\_turb} - T_a \cdot (P_s/P_a)^{R_{air}/C_p}\} \quad (1)$$

$$LE = \rho \cdot L_v \cdot C_{DE}(T_{s\_turb}) \cdot |\vec{V}| \cdot \{Q_{sat}(T_{s\_turb}) - Q_a\} \quad (2)$$

$$F_u = -\rho \cdot C_{DM}(T_{s\_turb}) \cdot |\vec{V}| \cdot U_a \quad (3)$$

$$F_v = -\rho \cdot C_{DM}(T_{s\_turb}) \cdot |\vec{V}| \cdot V_a \quad (4)$$

T_{s_turb} is surface temperature, SH is sensible heat flux, LE is latent heat flux, F_u and F_v are momentum fluxes, ρ is air density, C_p is specific heat of air at constant pressure, L_v is latent

heat of condensation, $C_{DH}(T_{s\_turb})$, $C_{DE}(T_{s\_turb})$, and $C_{DM}(T_{s\_turb})$ are aerodynamic transfer coefficients that are dependent on T_{s_turb}, $|\vec{V}|$ is surface wind speed, T_a is temperature at the lowest atmospheric layer, P_s is surface pressure, P_a is pressure at the lowest atmospheric layer, R_{air} is the gas constant of air, $Q_{sat}(T_{s\_turb})$ is saturation specific humidity that is dependent on T_{s_turb}, Q_a is specific humidity at the lowest atmospheric layer, U_a is westerly wind speed at the lowest atmospheric layer, V_a is southerly wind speed at the lowest atmospheric layer.

The turbulent fluxes, SH, LE, F_u, and F_v, are dependent on T_{s_turb}. Likewise, the turbulent transport of aerosol from the surface to the atmosphere is also dependent on T_{s_turb}. In the AMIP experiment, SST is used as an input variable T_{s_turb} to calculate the turbulent transport of sensible heat, latent heat, momentum, and aerosol from the sea surface. In the AMIP-p4Kturb experiment, we add 4K to T_{s_turb} at the sea surface. The experimental setting of the AMIP-p4Kturb is the same as the AMIP, other than adding 4K to T_{s_turb}. The 4K warming of T_{s_turb} causes an increase in SH and LE. As a result, both atmospheric temperature and specific humidity increase (blue curves in Figure 3gh).

Text S2. Response of latent heat flux to increasing longwave radiation from the sea surface

In AMIP-p4Krad experiment, upward longwave radiation from the sea surface increases relative to the AMIP experiment, which leads to a reduction in the surface latent heat flux, as shown in Figure S8(a). The decrease in the surface latent heat flux contributes to the decrease in specific humidity (Figure 3g, red). To better understand the mechanism of the decrease in surface latent heat flux, we decompose the response of the surface latent heat flux into contribution from multiple factors, as follows.

In MIROC5 and MIROC6, the latent heat flux is calculated according to the equation (2) in Text S1. Time-averaging the equation (2), and focusing on the difference between AMIP-p4Krad and AMIP experiments, we obtain

$$\Delta\overline{LE} = L_v \cdot \Delta\overline{\rho \cdot |\vec{V}| \cdot C_{DE}(T_{s\_turb}) \cdot DELQ} \qquad (5)$$

where $DELQ \equiv Q_{sat}(T_{s\_turb}) - Q_a$, $\overline{(\ \ )}$ is time-averaging, and Δ denotes AMIP-p4Krad minus AMIP experiment. We further rewrite the equation as

$$\Delta\overline{LE} = L_v \cdot \Delta\left\{\bar{\rho} \cdot \overline{|\vec{V}|} \cdot \overline{C_{DE}(T_{s\_turb})} \cdot \overline{DELQ}\right\} + residual \quad (6).$$

The magnitude of the residual in (6) depends on the period of time-averaging. Over the low latitude oceans, it is mostly of the order of 10 W/m^2 for monthly, 0.5 W/m^2 for daily, and 0.1 W/m^2 for 6 hourly averages. In the following, we use daily averaged data so that the residual in (6) becomes much smaller than $\Delta\overline{LE}$, that is greater than 4 W/m^2 in magnitude (Figure S8(a)). Neglecting the residual, we assume that the equation (6) can be approximated as

$$\Delta\overline{LE} \approx L_v \cdot \Delta\left\{\bar{\rho} \cdot \overline{|\vec{V}|} \cdot \overline{C_{DE}(T_{s\_turb})} \cdot \overline{DELQ}\right\} \qquad (7).$$

Using the 1st Taylor polynomial, the right hand side of (7) can be written as,

$$\begin{aligned}\Delta\overline{LE} \approx L_v \cdot & \left\{\overline{|\vec{V}|} \cdot \overline{C_{DE}(T_{s_{turb}})} \cdot \overline{DELQ}\right\}_{AMIP} \cdot \Delta\bar{\rho} \\ & + L_v \cdot \left\{\bar{\rho} \cdot \overline{C_{DE}(T_{s_{turb}})} \cdot \overline{DELQ}\right\}_{AMIP} \cdot \Delta\overline{|\vec{V}|} \\ & + L_v \cdot \left\{\bar{\rho} \cdot \overline{|\vec{V}|} \cdot \overline{DELQ}\right\}_{AMIP} \cdot \Delta\overline{C_{DE}(T_{s_{turb}})} \\ & + L_v \cdot \left\{\bar{\rho} \cdot \overline{|\vec{V}|} \cdot \overline{C_{DE}(T_{s\_turb})}\right\}_{AMIP} \cdot \Delta\overline{DELQ} + residual \quad (8)\end{aligned}$$

The changes in latent heat flux, $\Delta\overline{LE}$, are now decomposed into contribution from the changes in surface air density (the 1st term on the right hand side of (8)), surface wind speed (the 2nd term), bulk coefficient (the 3rd term), vertical contrast of specific humidity (the 4th term), and the residual. Each term in the equation (8) is calculated using the daily output from MIROC6, and the results are plotted in Figure S8. The figure shows that the decrease in latent heat flux, $\Delta\overline{LE}$, is mostly explained by the contribution from the changes in bulk coefficient (Figure S8ad). This result is consistent with the understanding that the longwave-induced warming of the atmosphere increases the static stability at the air-sea interface, which suppresses the turbulent transport of water vapor from the sea surface.

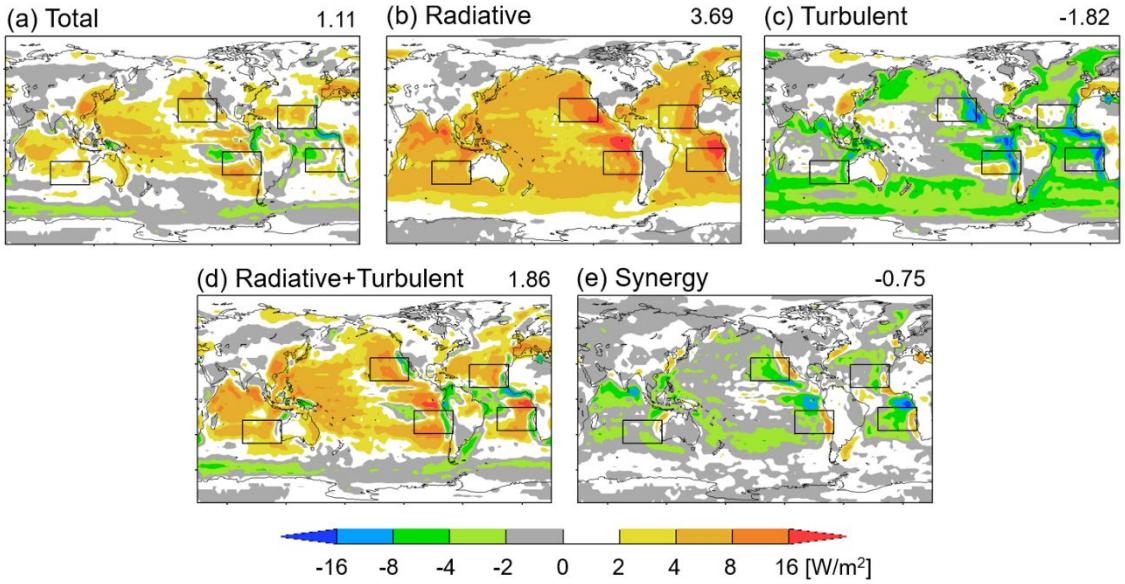

Figure S1. As in Figure 2, but the simulation data are created using MIROC5. Pattern correlation between (a) and (d) is 0.78.

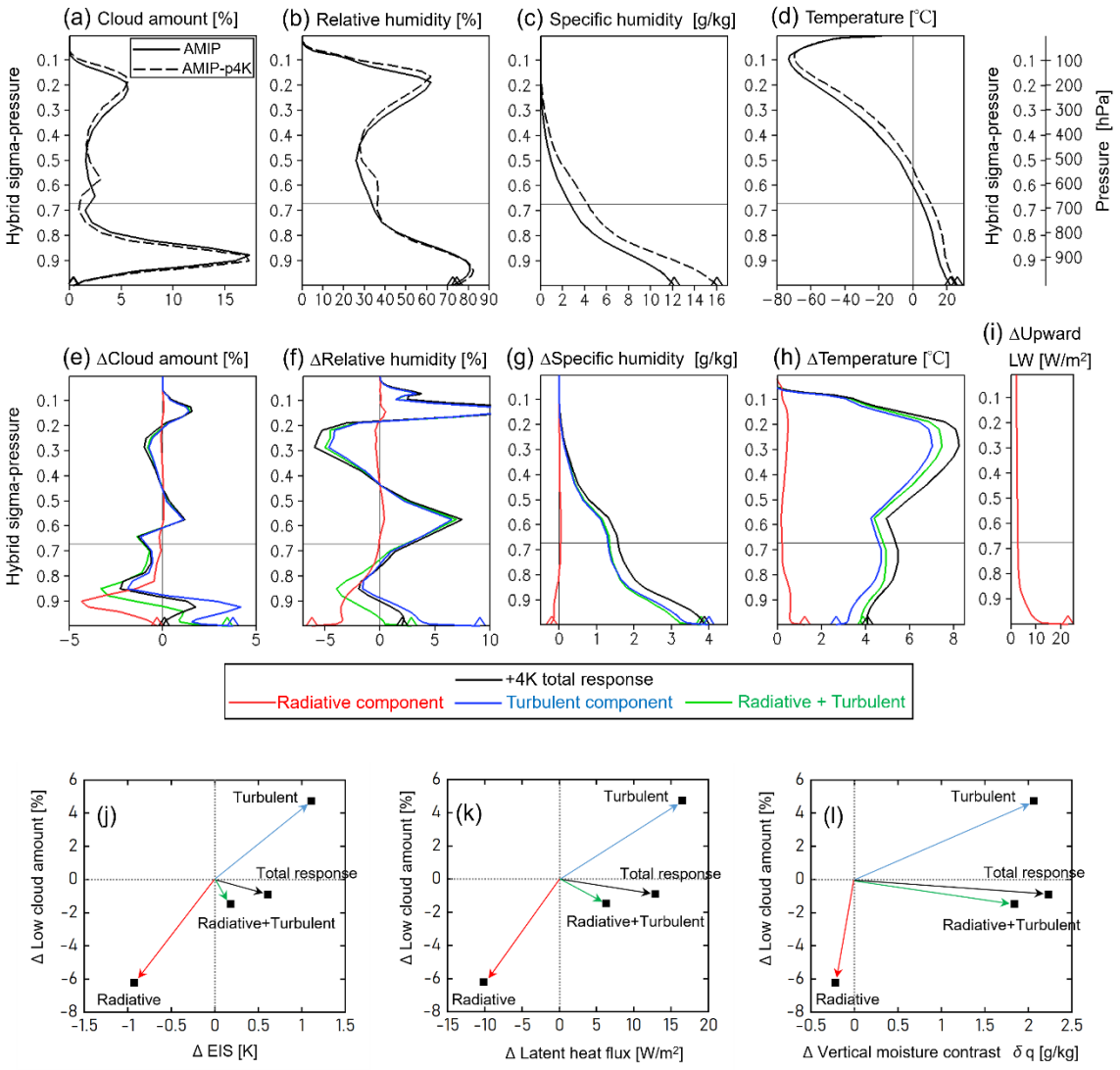

Figure S2. As in Figure 3, but the simulation data are created using MIROC5.

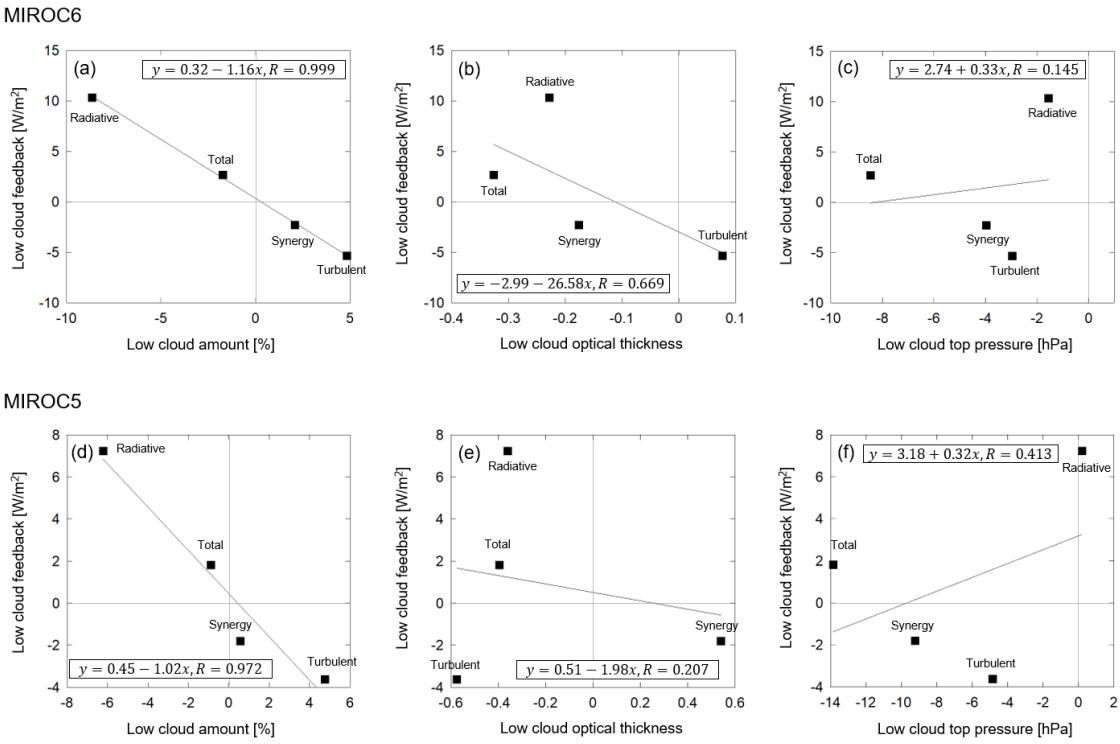

Figure S3. Relation between low cloud feedback and changes in (a)(d) low cloud amount, (b)(e) low cloud optical thickness, and (c)(f) low cloud top pressure, induced by SST+4K. The results are averages over the low cloud regions indicated by the black rectangles in Figure 2. The simulation data are created using (a)(b)(c) MIROC6 and (d)(e)(f) MIROC5. Regression equation and correlation coefficient are also shown in each panel.

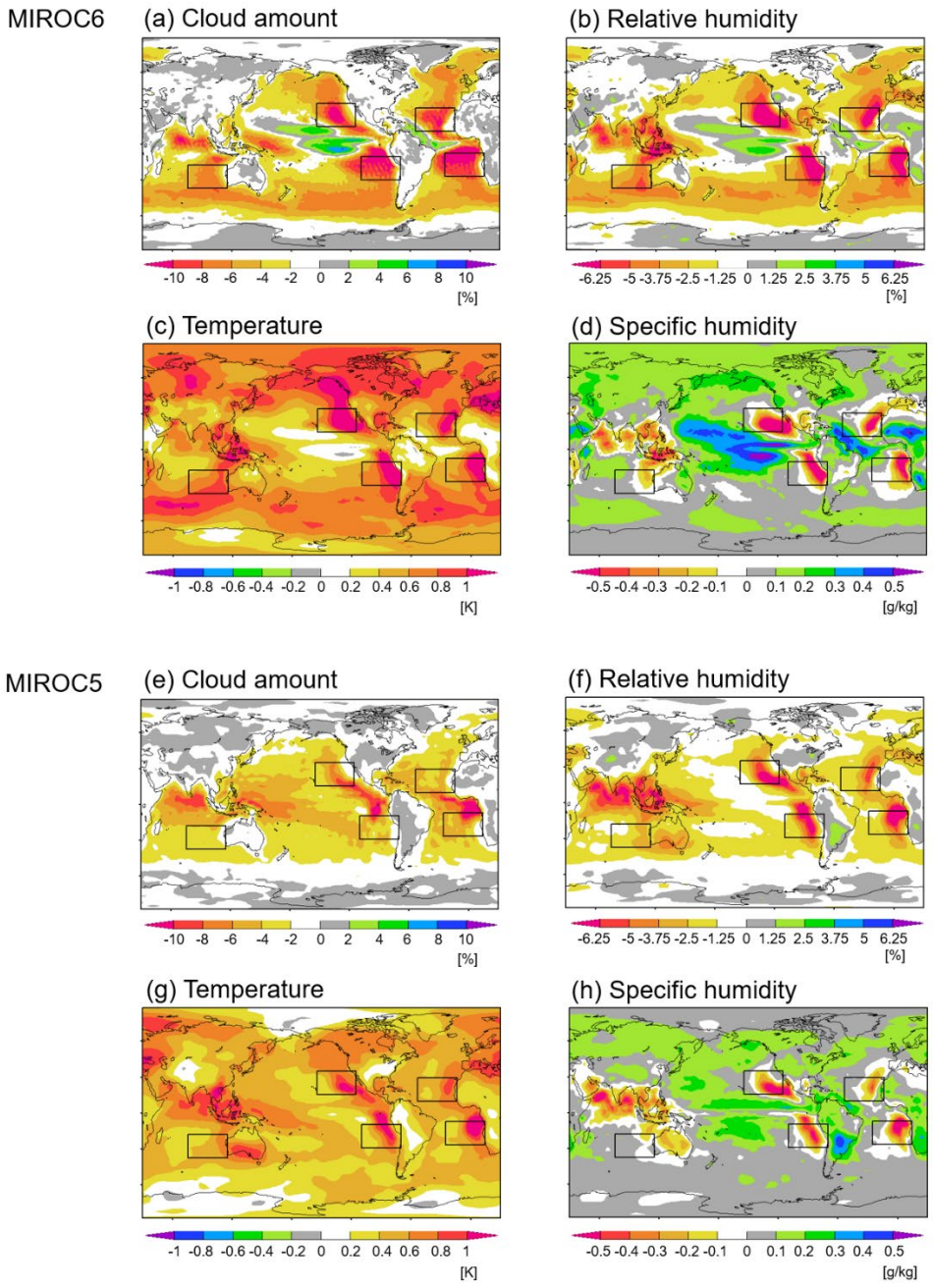

Figure S4. Radiative component of changes in (a)(e) cloud amount, (b)(f) relative humidity, (c)(g) temperature, and (d)(h) specific humidity, at the vertical σ-p level of 0.90. The simulation data are created using (a)(b)(c)(d) MIROC6 and (e)(f)(g)(h) MIROC5. Black rectangles indicate low cloud regions focused on in Figure 3.

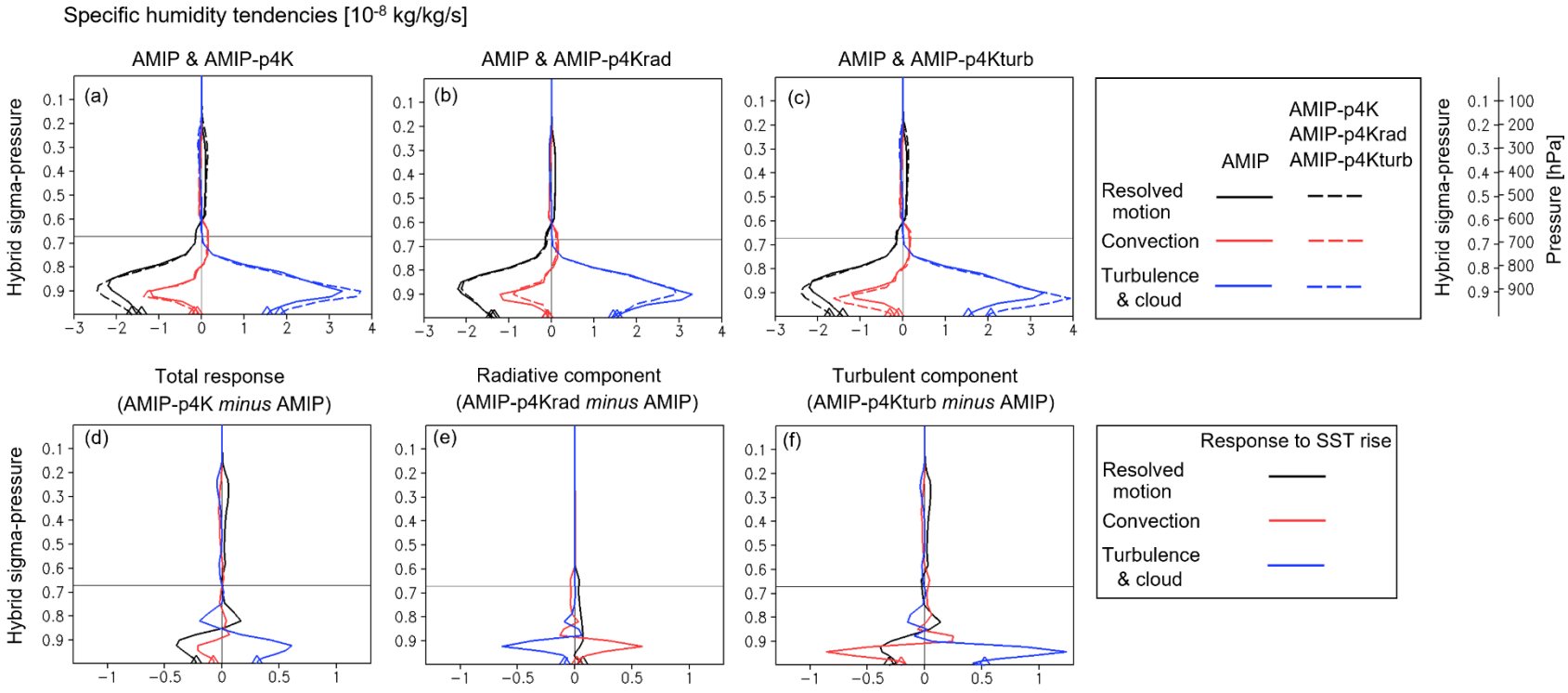

Figure S5. Specific humidity tendencies in (a) AMIP and AMIP-p4K, (b) AMIP and AMIP-p4Krad, and (c) AMIP and AMIP-p4Kturb experiments. Responses to SST +4K warming are also shown for (d) total response, (e) radiative component, and (f) turbulent component. The results are vertical profiles averaged over the low cloud regions indicated by the black rectangles in Figure 2. The vertical coordinate is hybrid σ-p on model level, which is compared with pressure levels on the top-right corner. The simulation data are created using MIROC6. Diamonds indicate values at the lowest level.

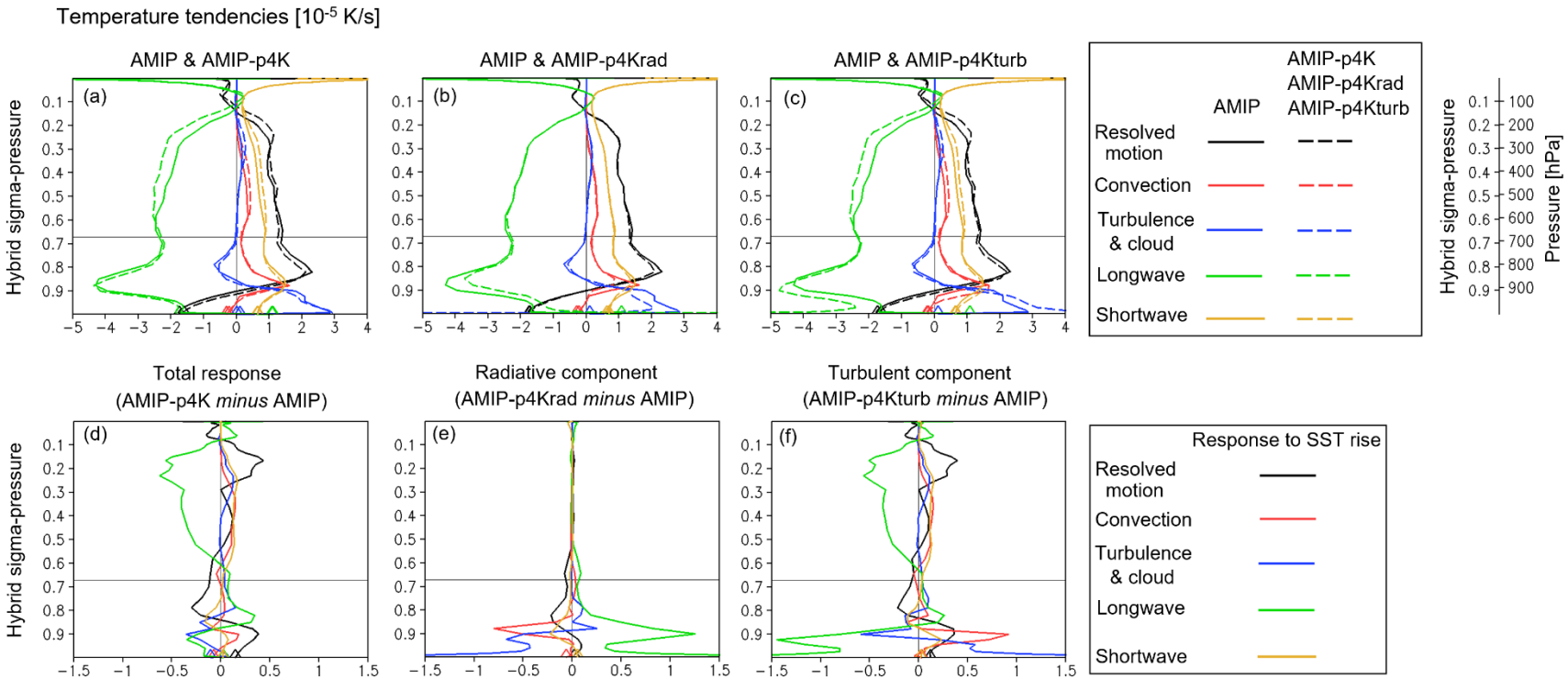

Figure S6. Temperature tendencies in (a) AMIP and AMIP-p4K, (b) AMIP and AMIP-p4Krad, and (c) AMIP and AMIP-p4Kturb experiments. Responses to SST +4K warming are also shown for (d) total response, (e) radiative component, and (f) turbulent component. The results are vertical profiles averaged over the low cloud regions indicated by the black rectangles in Figure 2. The vertical coordinate is hybrid σ-p on model level, which is compared with pressure levels on the top-right corner. The simulation data are created using MIROC6. Diamonds indicate values at the lowest level.

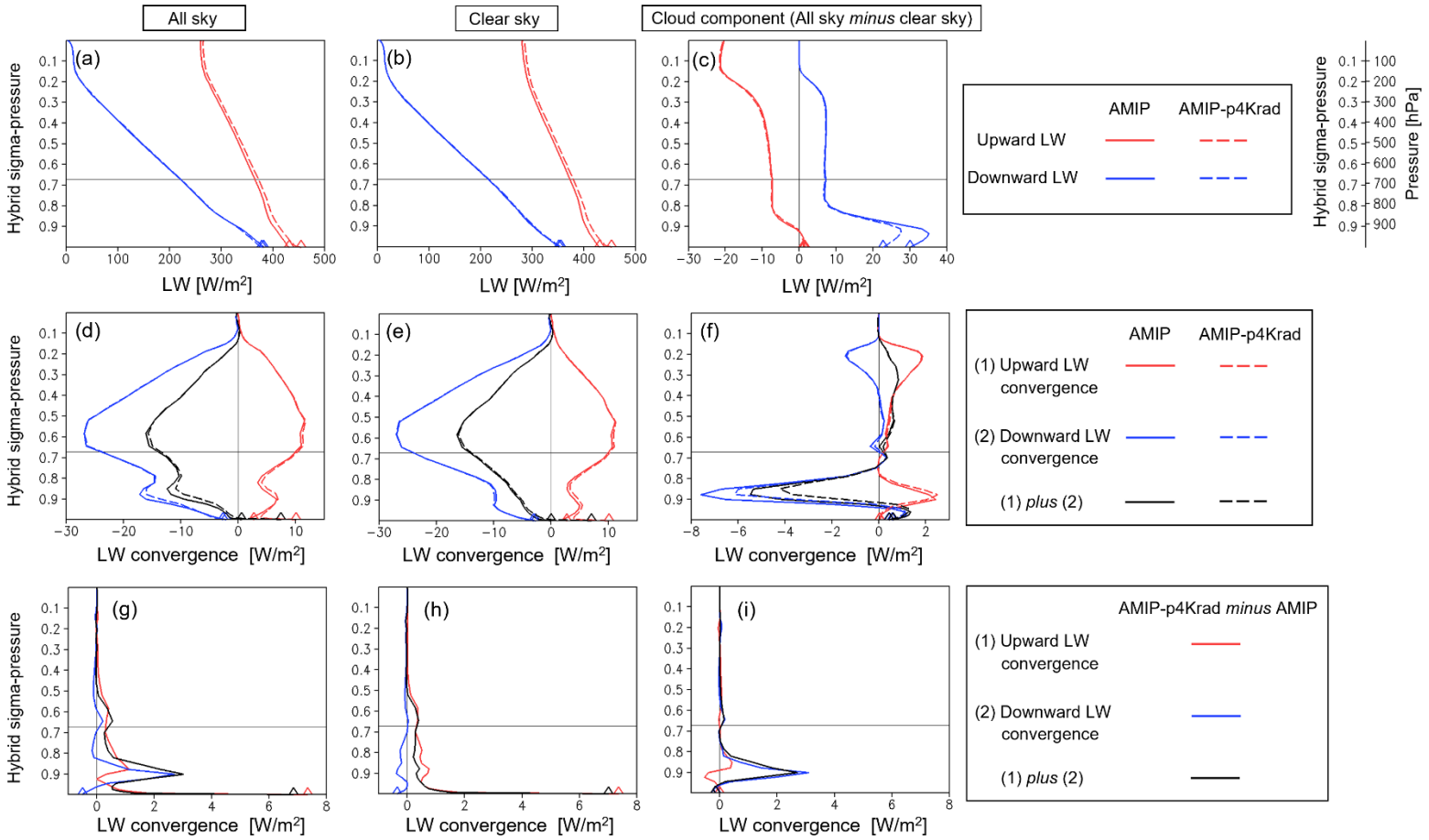

Figure S7. (a)(b)(c) Upward and downward longwave radiation, and (d)(e)(f) their vertical convergence in the AMIP and AMIP-p4Krad experiments. (g)(h)(i) Changes in the vertical convergence due to the SST warming in the AMIP-p4Krad experiment. Results are shown for (a)(d)(g) all sky, (b)(e)(h) clear sky, and (c)(f)(i) cloud component (all sky minus clear sky), averaged over the low cloud regions indicated by the black rectangles in Figure 2. The simulation data are created using MIROC6. Diamonds indicate values at the lowest level. The vertical coordinate is hybrid σ-p on model level, which is compared with pressure levels on the top-right corner.

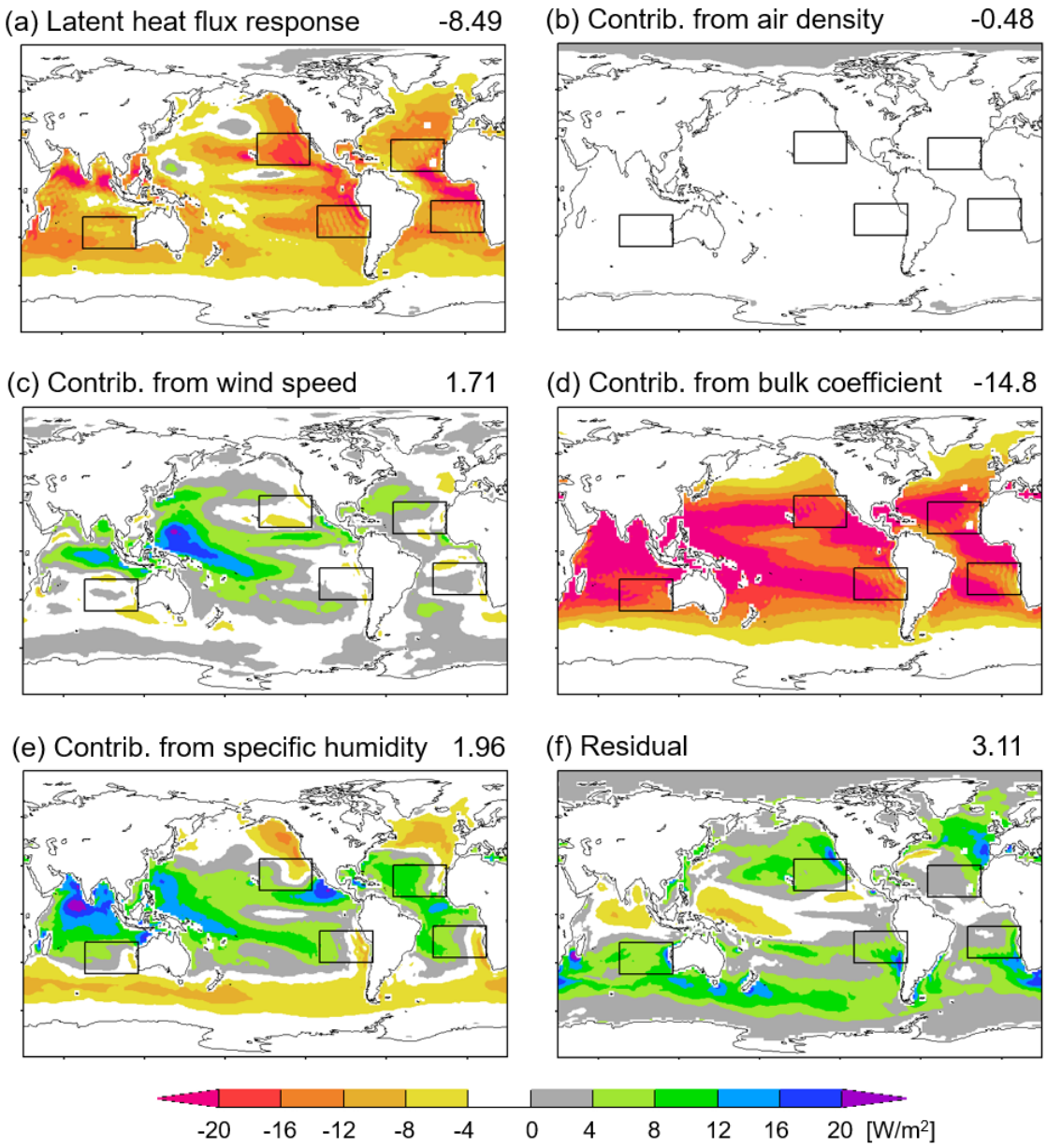

Figure S8. Changes in latent heat flux at the sea surface induced by SST warming of 4K. Results are shown for the radiative component, namely, AMIP-p4Krad minus AMIP. (a) changes in latent heat flux, (b) contribution to (a) from changes in surface air density, (c) contribution to (a) from changes in surface wind speed, (d) contribution to (a) from changes in bulk coefficient, (e) contribution to (a) from changes in vertical contrast of specific humidity, and (f) residual. Global averages are indicated at the top right of each panel. The simulation data are created using MIROC6. Definition of the quantities shown in panels (b)-(f) is given in Text S2.

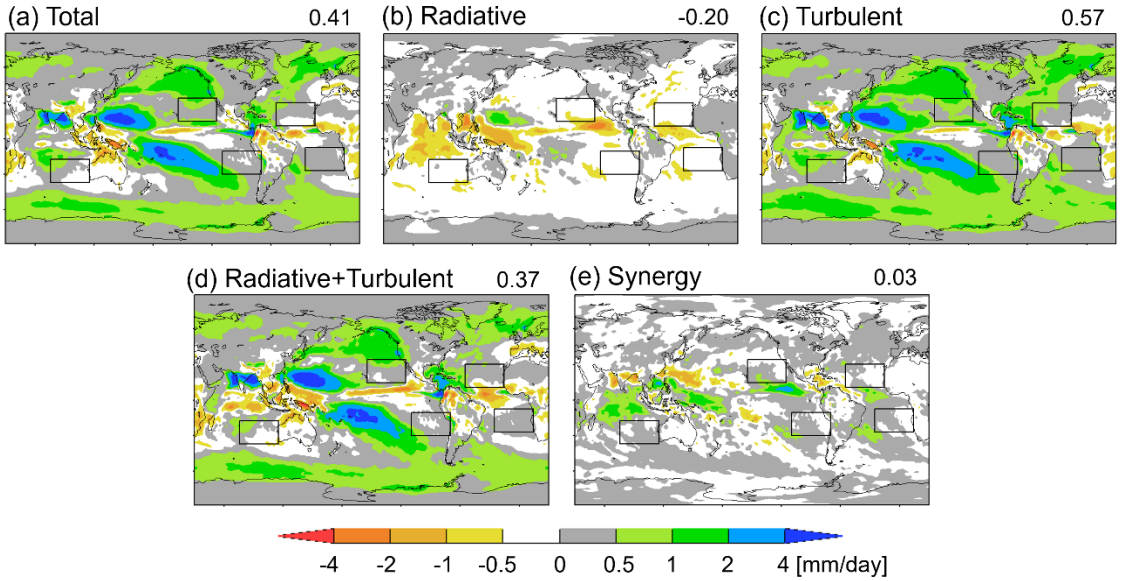

Figure S9. Response of precipitation to 4K increases in SST. (a) Total response, (b) radiative component, (c) turbulent component, (d) sum of the radiative and turbulent components, and (e) synergy. Global averages are indicated at the top right of each panel. Annual mean output from MIROC6 is presented.

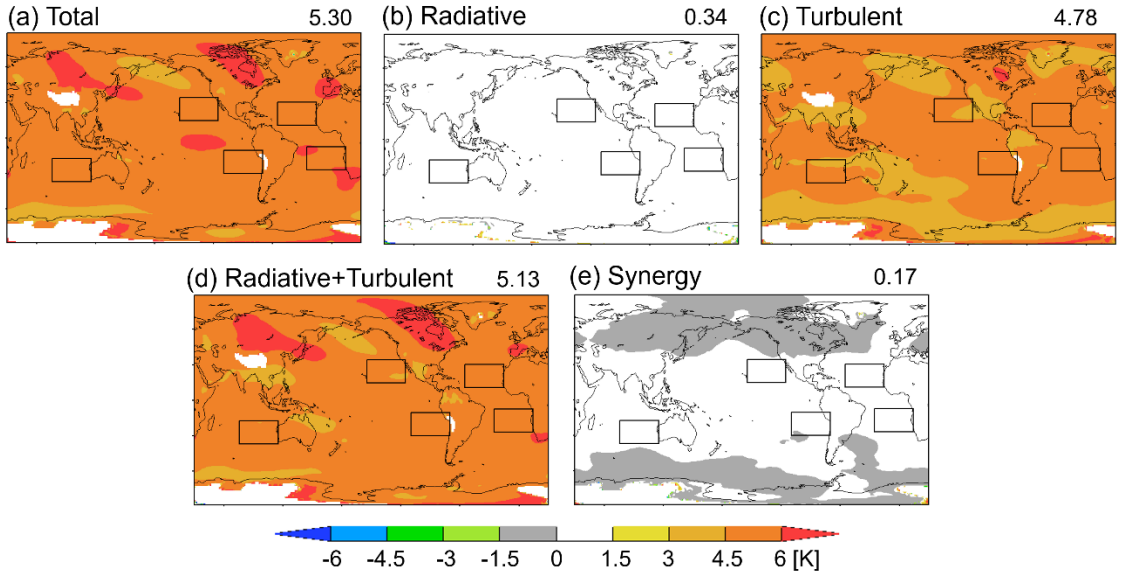

Figure S10. Response of temperature at 700hPa level to 4K increases in SST. (a) Total response, (b) radiative component, (c) turbulent component, (d) sum of the radiative and turbulent components, and (e) synergy. Global averages are indicated at the top right of each panel. Annual mean output from MIROC6 is presented.

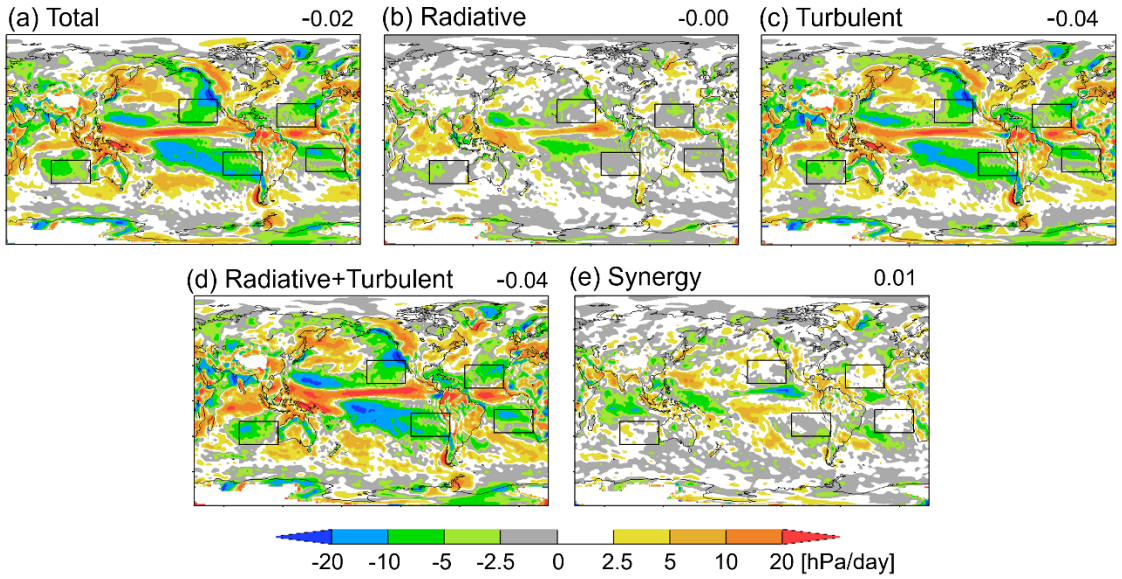

Figure S11. Response of vertical pressure velocity at 700hPa level to 4K increases in SST. (a) Total response, (b) radiative component, (c) turbulent component, (d) sum of the radiative and turbulent components, and (e) synergy. Positive sign indicates downward direction. Global averages are indicated at the top right of each panel. Annual mean output from MIROC6 is presented.

Table S1. Examples of low cloud feedback mechanisms and how they relate to the present study

Mechanism	Is the mechanism consistent with the results of the present study? Namely, can the mechanism explain the low cloud changes in AMIP-p4Krad or AMIP-p4Kturb compared to AMIP?
Positive feedback due to low cloud decrease (Rieck et al. 2012) In the trade wind cumulus regions, if large-scale atmospheric processes act to keep relative humidity constant, atmospheric warming induces an increase in surface moisture fluxes. This drives a deeper boundary layer and hence mixes more dry and warm air from the free troposphere to the surface. As a result, shallow cumulus layers tend to have fewer clouds.	Yes and No. Consistent with the low cloud decrease in AMIP-p4Kturb(σ -p$\approx$0.85). Not consistent with the low cloud decrease in AMIP-p4Krad, because there is no increase in surface evaporation (Fig.S8a). Not consistent with the low cloud increase in AMIP-p4Kturb (σ -p$\gtrsim$0.9).
Positive feedback due to low cloud decrease (Webb and Lock 2013) Global mean surface evaporation increases with global temperature rise. However, in the subtropical stratocumulus/trade cumulus transition regions, the increase in evaporation may be less than the global mean because the Walker circulation weakens, which reduces both the near-surface wind speed and the air-sea temperature difference, while the near-surface relative humidity increases. As a result, the supply of water vapor from surface evaporation does not increase enough to maintain the low level cloud fraction in the warmer climate.	Yes and No. Consistent with the low cloud decrease in AMIP-p4Kturb(σ -p$\approx$0.85). Consistent with the low cloud decrease in AMIP-p4Krad, because reduction of the near-surface wind speed contributes to the decrease in surface evaporation (Figs.S8a,c). Not consistent with the low cloud increase in AMIP-p4Kturb (σ -p$\gtrsim$0.9).
Positive feedback due to low cloud decrease (Bretherton et al. 2013, Tan et al. 2017, Schneider et al. 2019)	Yes and No. Consistent with the low cloud decrease in AMIP-p4Kturb(σ -

Over marine boundary-layer stratocumulus cloud, the warmer free troposphere contains more water vapor, hence is more emissive. This increases the downwelling radiation from the free troposphere and reduces the net radiative cooling of the cloud-topped boundary layer, reducing the turbulence production. As a result, the entrainment rate decreases at the cloud top, leading to a lowering of the inversion and a thinning of the cloud layer.	p≈0.85). Not consistent with the low cloud decrease in AMIP-p4Krad, because there is little increase in water vapor specific humidity in the free troposphere (red curve in Fig.3g). Not consistent with the low cloud increase in AMIP-p4Kturb (σ - p $\gtrsim$ 0.9).
Positive feedback due to low cloud decrease (Brient and Bony 2013) In a warmer climate, the non-linearity of the Clausius-Clapeyron relationship leads to a larger increase in specific humidity at high temperatures and low altitudes than at lower temperatures and higher altitudes. This leads to an enhanced vertical gradient of specific humidity and moist static energy (MSE) between the boundary layer and the lower free troposphere, and thus an enhanced import of low-MSE and dry air from the free troposphere down to the surface by large-scale subsidence. This decreases the low-level cloud fraction.	Yes and No. Consistent with the low cloud decrease in AMIP-p4Kturb(σ - p≈0.85). Not consistent with the low cloud decrease in AMIP-p4Krad, because there is no increase in vertical gradient of specific humidity (red curve in Fig.3g). Not consistent with the low cloud increase in AMIP-p4Kturb (σ - p $\gtrsim$ 0.9).
Positive feedback due to low cloud decrease (Zhang et al. 2013, Brient et al. 2016, Vial et al. 2016). Higher SST causes a warmer climate, with a larger moisture contrast between the free troposphere and the boundary layer. The larger moisture contrast enhances the upward moisture flux by shallow convection or cloud-top entrainment at the level immediately above the top of the	Yes and No. Consistent with the low cloud decrease in AMIP-p4Kturb(σ - p≈0.85). Not consistent with the low cloud decrease in AMIP-p4Krad, because there is no increase in vertical moisture contrast (red curve in Fig.3g).

boundary layer. This causes larger ventilation of the cloud layer, which tends to decrease low cloud. The decrease in low cloud is accompanied by a reduction of radiative cooling by the low cloud. As a result, lower troposphere becomes stabilized. This weakens the latent heat flux from the sea surface, reducing the low cloud further.	Not consistent with the low cloud increase in AMIP-p4Kturb (σ -p $\gtrsim$ 0.9).
Positive feedback due to low cloud decrease (Vogel et al. 2019) In the downstream trade cumulus regions, sea surface warming leads to an increase in the surface fluxes, which deepens the shallow convection and increases precipitation. The increase in precipitation leads to a reduction of the detrained stratiform layers. In addition, the deeper clouds penetrate the inversion and detrain the moisture in the free troposphere, which further reduces the stratiform cloudiness.	No. Not consistent with AMIP-p4Krad or AMIP-p4Kturb, because low clouds do not deepen in either of the experiments compared to AMIP.
Negative feedback due to low cloud increase (Miller 1997, Klein and Hartmann 1993, Wood and Bretherton 2006, Qu et al. 2015, Tan et al. 2016) In low latitudes, the free-tropospheric temperature profile stabilizes with global warming. This increases the strength of the inversion capping the planetary boundary layer. As a result, vertical mixing across the inversion reduces, keeping the boundary layer shallower and more humid, which increases the stratiform low cloud cover.	Yes and No. Consistent with the low cloud decrease in AMIP-p4Krad, because the strength of the inversion decreases with warming (red curve in Fig3h). Consistent with the low cloud increase in AMIP-p4Kturb (σ -p $\gtrsim$ 0.9), because the strength of the inversion increases with warming (blue curve in Fig3h). Not consistent with the low cloud decrease in AMIP-p4Kturb(σ -p$\approx$0.85).
Negative feedback due to low cloud increase (Wyant et al. 2009,	Yes and No.

Narenpitak and Bretherton 2019). Higher SST causes a warmer and moister trade-cumulus boundary layer which experiences stronger net radiative cooling. The stronger cooling destabilizes the cumulus layer, leading to more vigorous convection. This fosters a moister boundary layer with more cumulus clouds, which amplifies the anomalous radiative cooling.	 Consistent with the low cloud increase in AMIP-p4Kturb (σ -p $\gtrsim$ 0.9). Not consistent with the low cloud decrease in either AMIP-p4Krad or AMIP-p4Kturb (σ -p$\approx$0.85).
Negative feedback due to low cloud increase (Myers and Norris 2013) In the tropics, the atmospheric overturning circulation weakens as the climate warms. This leads to less subsidence over the subtropical marine boundary layer clouds, which allows a deeper inversion with more vertical development of the clouds, thickening the cloud layer.	No. Not consistent with AMIP-p4Krad or AMIP-p4Kturb, because low clouds do not deepen in either of the experiments compared to AMIP.
Negative feedback due to low cloud increase (Zhang et al. 2013). Higher SST causes a warmer climate. Accompanied by the weaker large-scale subsidence, the warmer climate has greater surface latent heat flux, larger turbulence moisture convergence in the cloud layer, and consequently an increase in low cloud.	Yes and No. Consistent with the low cloud increase in AMIP-p4Kturb (σ -p $\gtrsim$ 0.9). Not consistent with the low cloud decrease in either AMIP-p4Krad or AMIP-p4Kturb (σ -p$\approx$0.85).

References

Bretherton, C. S., P. N. Blossey, and C. R. Jones (2013), Mechanisms of marine low cloud sensitivity to idealized climate perturbations: A single-LES exploration extending the CGILS cases, J. Adv. Model. Earth Syst., 5, 316-337, doi:10.1002/jame.20019.

Brient, F. and S. Bony (2013), Interpretation of the positive low-cloud feedback predicted by a climate model under global warming, Clim. Dyn., 40, 2415-2431, doi:10.1007/s00382-011-1279-7.

Brient, F., T. Schneider, Z. Tan, S. Bony, X. Qu, and A. Hall (2016), Shallowness of tropical low clouds as a predictor of climate models' response to warming, Clim. Dyn., 47, 433-449, doi:10.1007/s00382-015-2846-0.

Klein, S. A. and D. L. Hartmann (1993), The seasonal cycle of low stratiform clouds, J. Clim., 6, 1587-1606.

Miller, R. L. (1997), Tropical thermostats and low cloud cover, J. Clim., 10, 409-440.

Myers, T. A. and J. R. Norris (2013), Observational evidence that enhanced subsidence reduces subtropical marine boundary layer cloudiness, J. Clim., 26, 7507-7524, doi:10.1175/JCLI-D-12-00736.1.

Narenpitak, P., and C. S. Bretherton (2019), Understanding negative subtropical shallow cumulus cloud feedbacks in a near-global aquaplanet model using limited area cloud-resolving simulations, J. Adv. Model. Earth Syst., 11, 1600-1626, doi:10.1029/2018MS001572.

Qu, X., A. Hall, S. A. Klein, and P. M. Caldwell (2015), The strength of the tropical inversion and its response to climate change in 18 CMIP5 models, Clim. Dyn., 45, 375-396, doi:10.1007/s00382-014-2441-9.

Rieck, M., L. Nuijens, and B. Stevens (2012), Marine boundary layer cloud feedbacks in a constant relative humidity atmosphere, J. Atmos. Sci., 69, 2538-2550, doi:10.1175/JAS-D-11-0203.1.

Schneider, T., C. M. Kaul, and K. G. Pressel (2019), Possible climate transitions from breakup of stratocumulus decks under greenhouse warming, Nat. Geosci., 12, 163-167, doi:10.1038/s41561-019-0310-1.

Tan, Z., T. Schneider, J. Teixeira, and K. G. Pressel (2016), Large-eddy simulation of subtropical cloud-topped boundary layers: 1. A forcing framework with closed surface energy balance, J. Adv. Model. Earth Syst., 8, 1565-1585, doi:10.1002/2016MS000655.

Tan, Z., T. Schneider, J. Teixeira, and K. G. Pressel (2017), Large-eddy simulation of subtropical cloud-topped boundary layers: 2. Cloud response to climate change, J. Adv. Model. Earth Syst., 9, 19-38, doi:10.1002/2016MS000804.

Vial, J., S. Bony, J.-L. Dufresne, and R. Roehrig (2016), Coupling between lower-tropospheric convective mixing and low-level clouds: Physical mechanisms and dependence on convection scheme, J. Adv. Model. Earth Syst., 8, 1892-1911, doi:10.1002/2016MS000740.

Vogel, R., L. Nuijens, and B. Stevens (2019), Influence of deepening and mesoscale organization of shallow convection on stratiform cloudiness in the downstream trades, Q. J. R. Meteorol. Soc., 146, 174-185, doi:10.1002/qj.3664.

Webb, M. J. and A. P. Lock (2013), Coupling between subtropical cloud feedback and the local hydrological cycle in a climate model, Clim. Dyn., 41, 1923-1939, doi:10.1007/s00382-012-1608-5.

Wood, R. and C. S. Bretherton (2006), On the relationship between stratiform low cloud cover and lower-tropospheric stability, J. Clim., 19, 6425-6432, doi:10.1175/JCLI3988.1.

Wyant, M. C., C. S. Bretherton, and P. N. Blossey (2009), Subtropical low cloud response to a warmer climate in a superparameterized climate model. Part 1: Regime sorting and physical mechanisms, J. Adv. Model. Earth Syst., 1, 7, doi:10.3894/JAMES.2009.1.7.

Zhang, M., C. S. Bretherton, P. N. Blossey, P. H. Austin, J. T. Bacmeister, S. Bony, F. Brient, S. K. Cheedela, A. Cheng, A. D. Del Genio, S. R. De Roode, S. Endo, C. N. Franklin, J.-C. Golaz, C. Hannay, T. Heus, F. A. Isotta, J.-L. Dufresne, I.-S. Kang, H. Kawai, M. Köehler, V. E. Larson, Y. Liu, A. P. Lock, U. Lohmann, M. F. Khairoutdinov, A. M. Molod, R. A. J. Neggers, P. Rasch, I. Sandu, R. Senkbeil, A. P. Siebesma, C. Siegenthaler-Le Drian, B. Stevens, M. J. Suarez, K.-M. Xu, K. von Salzen, M. J. Webb, A. Wolf, and M. Zhao (2013), CGILS: Results from the first phase of an international project to understand the physical mechanisms of low cloud feedbacks in single column models, J. Adv. Model. Earth Syst., 5, 1-17, doi:10.1002/2013MS000246.